

<sup>1</sup> **Cross-scale interaction of host tree size and climate governs bark  
2 beetle-induced tree mortality**

<sup>3</sup> Michael J. Koontz<sup>1,2,3\*</sup>, Andrew M. Latimer<sup>1,2</sup>, Leif A. Mortenson<sup>4</sup>, Christopher J. Fettig<sup>5</sup>, Malcolm P.  
<sup>4</sup> North<sup>1,2,6</sup>

<sup>5</sup> <sup>1</sup>Graduate Group in Ecology, University of California, Davis, CA, USA

<sup>6</sup> <sup>2</sup>Department of Plant Sciences, University of California, Davis, CA, USA

<sup>7</sup> <sup>3</sup>Earth Lab, University of Colorado-Boulder; Boulder, CO, USA

<sup>8</sup> <sup>4</sup>USDA Forest Service, Pacific Southwest Research Station, Placerville, CA, USA

<sup>9</sup> <sup>5</sup>USDA Forest Service, Pacific Southwest Research Station, Davis, CA, USA

<sup>10</sup> <sup>6</sup>USDA Forest Service, Pacific Southwest Research Station, Mammoth Lakes, CA, USA

<sup>11</sup> \*Correspondence: michael.koontz@colorado.edu

<sup>12</sup> *Keywords:* *Dendroctonus brevicomis*, disturbance, drones, *Pinus ponderosa*, Sierra Nevada, structure from motion, forest structure, climate change-type drought, macroecology

<sup>14</sup> *Abstract word count:* 348

<sup>15</sup> *Overall .docx word count:* 12959

<sup>16</sup> *Main text word count:* 4684 (Intro: 1536; Results: 456 (45+119+292); Discussion: 2692)

<sup>17</sup> *Methods word count:* 2903 (697+642+1564)

<sup>18</sup> *Text boxes word count:* 0

<sup>19</sup> Date report generated: May 06, 2020

<sup>20</sup> **Abstract**

<sup>21</sup> The Californian hot drought of 2012 to 2015 created favorable conditions for unprecedented ponderosa pine  
<sup>22</sup> (*Pinus ponderosa*) mortality in the Sierra Nevada mountain range, largely attributable to the western pine  
<sup>23</sup> beetle (*Dendroctonus brevicomis*; WPB). Climate conditions can partially explain tree mortality patterns  
<sup>24</sup> through their direct effect on tree vigor, but tree mortality rates can respond non-linearly to climate  
<sup>25</sup> conditions when bark beetles interact with local forest characteristics while they colonize drought-stressed  
<sup>26</sup> trees. Measuring broad-scale climate conditions simultaneously with local forest composition and structure–  
<sup>27</sup> the spatial distribution and size of trees– will refine our understanding of how these variables interact, but  
<sup>28</sup> is generally expensive and/or labor-intensive. We use drone surveys over 32 distinct sites along a 350-km  
<sup>29</sup> latitudinal and 1000-m elevational gradient in western slope Sierra Nevada ponderosa pine/mixed-conifer

30 forests and structure from motion (SfM) photogrammetry to segment and classify more than 450,000 trees  
31 over 9 km<sup>2</sup> of forest with WPB-induced tree mortality. We validated the segmentation and classification  
32 with data from 160 coincident field plots (each 0.041 ha in area) throughout the 32 sites, assuming that dead  
33 trees were all ponderosa pine killed by WPB. We modeled the probability of ponderosa pine mortality as a  
34 function of forest structure and composition and their interaction with site-level climatic water deficit (CWD),  
35 accounting for spatial covariance using exact Gaussian processes. A greater local proportion of host trees  
36 strongly increased the probability of host mortality, with greater host density amplifying this effect. Further,  
37 we found a strong interaction between host size and CWD such that larger trees increased the probability of  
38 host mortality at hot/dry sites, but smaller trees tended to drive mortality in cool/wet sites. Our results  
39 demonstrate a variable response of WPB to local forest structure and composition across an environmental  
40 gradient, which may help reconcile differences between observed ecosystem-wide tree mortality patterns and  
41 predictions from models based on coarser-scale forest structure. Climate change adaptation strategies should  
42 consider that future disturbance outcomes may depend on interactions between local forest structure and  
43 broad-scale environmental gradients, with the potential for cross-scale interactions that challenge our current  
44 understanding of forest insect dynamics.

## 45 **Introduction**

46 Bark beetles dealt the final blow to many of the nearly 150 million trees killed in the California hot drought of  
47 2012 to 2015 and its aftermath (USDAFS 2019). A harbinger of climate change effects to come, record high  
48 temperatures exacerbated the drought (Griffin and Anchukaitis 2014, Robeson 2015), which increased water  
49 stress in trees (Asner et al. 2016, Brodrick and Asner 2017), making them more susceptible to colonization  
50 by bark beetles (Fettig 2012, Kolb et al. 2016). Further, a century of fire suppression has enabled forests to  
51 grow into dense stands, which can also make them more vulnerable to bark beetles (Waring and Pitman  
52 1985, Fettig 2012, Restaino et al. 2019). This combination of environmental conditions and forest structural  
53 characteristics led to tree mortality events of unprecedented size across the state (Young et al. 2017, USDAFS  
54 2017).

55 Tree mortality exhibited a strong latitudinal and elevational gradient (Asner et al. 2016, Young et al. 2017)  
56 that can only be partially explained by coarse-scale measures of environmental conditions (i.e., historic  
57 climatic water deficit; CWD) and current forest structure (i.e., current regional basal area) (Young et al.  
58 2017). Progressive loss of canopy water content offers additional insight into tree vulnerability to mortality,  
59 but cannot ultimately resolve which trees die in forests with bark beetles as a key mortality agent (Brodrick  
60 and Asner 2017). Bark beetles respond to local forest characteristics in positive feedbacks that non-linearly

61 alter tree mortality dynamics against a background of environmental conditions that stress trees (Raffa et al.  
62 2008, Boone et al. 2011). Thus, an explicit consideration of local forest structure and composition (Stephenson  
63 et al. 2019, Fettig et al. 2019) as well as its cross-scale interaction with regional climate conditions (Senf  
64 et al. 2017) can refine our understanding of tree mortality patterns from California's recent hot drought.  
65 The challenge of simultaneously measuring the effects of both local-scale forest features (such as structure  
66 and composition) and broad-scale environmental conditions (such as climatic water deficit; CWD) on forest  
67 insect disturbance leaves their interaction effect relatively underexplored (Seidl et al. 2016, Senf et al. 2017,  
68 Stephenson et al. 2019, Fettig et al. 2019).

69 The ponderosa pine/mixed-conifer forests in California's Sierra Nevada region are characterized by regular  
70 bark beetle disturbances, primarily by the influence of western pine beetle (*Dendroctonus brevicomis*; WPB)  
71 on its host ponderosa pine (*Pinus ponderosa*) (Fettig 2016). WPB is a primary bark beetle— its reproductive  
72 success is contingent upon host tree mortality, which itself requires enough beetles to mass attack the host tree  
73 and overwhelm its defenses (Raffa and Berryman 1983). This Allee effect creates a strong coupling between  
74 beetle selection behavior of host trees and host tree susceptibility to colonization (Raffa and Berryman 1983,  
75 Logan et al. 1998, Wallin and Raffa 2004). A key defense mechanism of conifers to bark beetle attack is to  
76 flood beetle bore holes with resin, which physically expels colonizing beetles, can be toxic to the colonizers  
77 and their fungi, and may interrupt beetle communication (Franceschi et al. 2005, Raffa et al. 2015). Under  
78 normal conditions, weakened trees with compromised defenses are the most susceptible to colonization and  
79 will be the main targets of primary bark beetles like WPB (Bentz et al. 2010, Boone et al. 2011, Raffa et al.  
80 2015). Under severe water stress, many trees no longer have the resources available to mount a defense (Boone  
81 et al. 2011, Kolb et al. 2016) and thus prolonged drought can often trigger increased bark beetle-induced  
82 tree mortality as average tree vigor declines (Bentz et al. 2010) (though we note that the inciting factors  
83 for increased tree mortality in other bark beetle systems, such as mountain pine beetle (*D. ponderosae*) in  
84 lodgepole pine (*P. contorta*), may be more related to temperature's effect on the beetle's physiology). As  
85 the local population density of beetles increases due to successful reproduction within spatially-aggregated  
86 weakened trees, as might occur during drought, mass attacks grow in size and become capable of overwhelming  
87 formidable tree defenses such that even healthy trees may be susceptible to colonization and mortality (Bentz  
88 et al. 2010, Boone et al. 2011, Raffa et al. 2015). Thus, water stress can be a key determinant of whether  
89 individual trees are susceptible to bark beetles under many conditions, and this environmental condition may  
90 interact with beetle population dynamics to drive tree susceptibility under extreme conditions (Bentz et al.  
91 2010, Boone et al. 2011, Stephenson et al. 2019).

92 WPB activity is strongly influenced by forest structure— the spatial distribution and size of trees— and tree

93 species composition. Taking forest structure alone, high-density forests are more prone to bark beetle-induced  
94 tree mortality (Fettig 2012) which may arise as greater competition for water resources amongst crowded trees  
95 and thus average tree resistance is lower (Hayes et al. 2009), or because smaller gaps between trees protect  
96 pheromone plumes from dissipation by the wind and thus enhance intraspecific beetle communication (Thistle  
97 et al. 2004). Tree size is another aspect of forest structure that affects bark beetle host selection behavior  
98 with smaller trees tending to have lower capacity for resisting attack, and larger trees being more desirable  
99 targets on account of their thicker phloem providing greater nutritional content (Miller and Keen 1960,  
100 Chubaty et al. 2009, Boone et al. 2011, Graf et al. 2012). Throughout an outbreak, some bark beetle species  
101 will collectively “switch” the preferred size of tree to attack in order to navigate the trade-off between host  
102 susceptibility and host quality (Geiszler and Gara 1978, Klein et al. 1978, Mitchell and Preisler 1991, Preisler  
103 1993, Wallin and Raffa 2004). Taking forest composition alone, WPB activity in the Sierra Nevada mountain  
104 range of California is necessarily tied to the regional distribution of its exclusive host, ponderosa pine (Fettig  
105 2016). Colonization by primary bark beetles can also depend on the relative frequencies of tree species in a  
106 more local area, akin to reduced oligophagous insect herbivory in forests comprising taxonomically-distinct  
107 tree species compared to monocultures (Jactel and Brockerhoff 2007).

108 The interaction between forest structure and composition also drives WPB activity. For instance, dense forests  
109 with high host availability may experience greater beetle-induced tree mortality because dispersal distances  
110 between potential host trees are shorter reducing predation of adults searching for hosts and facilitating  
111 higher rates of colonization (Miller and Keen 1960, Berryman 1982, Fettig et al. 2007), or because high host  
112 availability reduces the chance of individual beetles wasting their limited resources flying to and landing  
113 on a non-host tree (Moeck et al. 1981, Evenden et al. 2014). Stand-scale measures of forest structure and  
114 composition thus paint a fundamentally limited picture of the mechanisms by which these forest characteristics  
115 affect bark beetle disturbance, but finer-grain information explicitly recognizing tree species, size, and local  
116 density should better capture the ecological processes underlying insect-induced tree mortality (Geiszler  
117 and Gara 1978, Mitchell and Preisler 1991, Preisler 1993, Kaiser et al. 2013). Additionally, considering the  
118 effects of local forest structure and composition with the effects of environmental conditions may help refine  
119 our understanding of tree mortality patterns in widespread events, such as during the recent California hot  
120 drought.

121 The vast spatial extent of tree mortality in the 2012 to 2015 California hot drought challenges our ability to  
122 simultaneously consider how broad-scale environmental conditions may interact with local forest structure  
123 and composition to affect the dynamic between bark beetle selection and colonization of host trees, and host  
124 tree susceptibility to attack (Anderegg et al. 2015, Stephenson et al. 2019). Measuring local forest structure

125 generally requires expensive instrumentation (Kane et al. 2014, Asner et al. 2016) or labor-intensive field  
126 surveys (Larson and Churchill 2012, Stephenson et al. 2019, Fettig et al. 2019), which constrains survey  
127 extent and frequency. Small, unhumanned aerial systems (sUAS) enable relatively fast and cheap remote  
128 imaging over hundreds of hectares of forest, which can be used to measure complex forest structure and  
129 composition at the individual tree scale with Structure from Motion (SfM) photogrammetry (Morris et al.  
130 2017, Shiklomanov et al. 2019). The ultra-high resolution of sUAS-derived measurements as well as the  
131 ability to incorporate vegetation reflectance can help overcome challenges in species classification and dead  
132 tree detection inherent in other remote sensing methods, such as airborne LiDAR (Jeronimo et al. 2019).  
133 Distributing such surveys across an environmental gradient can overcome the data acquisition challenge  
134 inherent in investigating phenomena with both a strong local- and a strong broad-scale component.

135 We used sUAS-derived remote sensing images over a network of 32 sites in Sierra Nevada ponderosa pine/mixed-  
136 conifer forests spanning 1000 m of elevation and 350 km of latitude (see Fettig et al. 2019) covering a total of  
137 9 km<sup>2</sup>, to investigate how broad-scale environmental conditions interacted with local forest structure and  
138 composition to shape patterns of tree mortality during the cumulative tree mortality event of 2012 to 2018.

139 We asked:

- 140 1. How does the proportion of host trees in a local area and average host tree size affect WPB-induced  
141 tree mortality?
- 142 2. How does the density of all tree species (hereafter “overall density”) affect WPB-induced tree mortality?
- 143 3. How does the total basal area of all tree species (hereafter “overall basal area”) affect WPB-induced  
144 tree mortality?
- 145 4. How does environmentally-driven tree moisture stress affect WPB-induced tree mortality?
- 146 5. Do the effects of forest structure, forest composition, and environmental condition interact to influence  
147 WPB-induced tree mortality?

## 148 Methods

### 149 Study system

150 We built our study coincident with 160 vegetation/forest insect monitoring plots at 32 sites established  
151 between 2016 and 2017 by Fettig et al. (2019) (Figure 1). The study sites were chosen to reflect typical  
152 west-side Sierra Nevada yellow pine/mixed-conifer forests and were dominated by ponderosa pine (Fettig  
153 et al. 2019). Plots were located in WPB-attacked, yellow pine/mixed-conifer forests across the Eldorado,

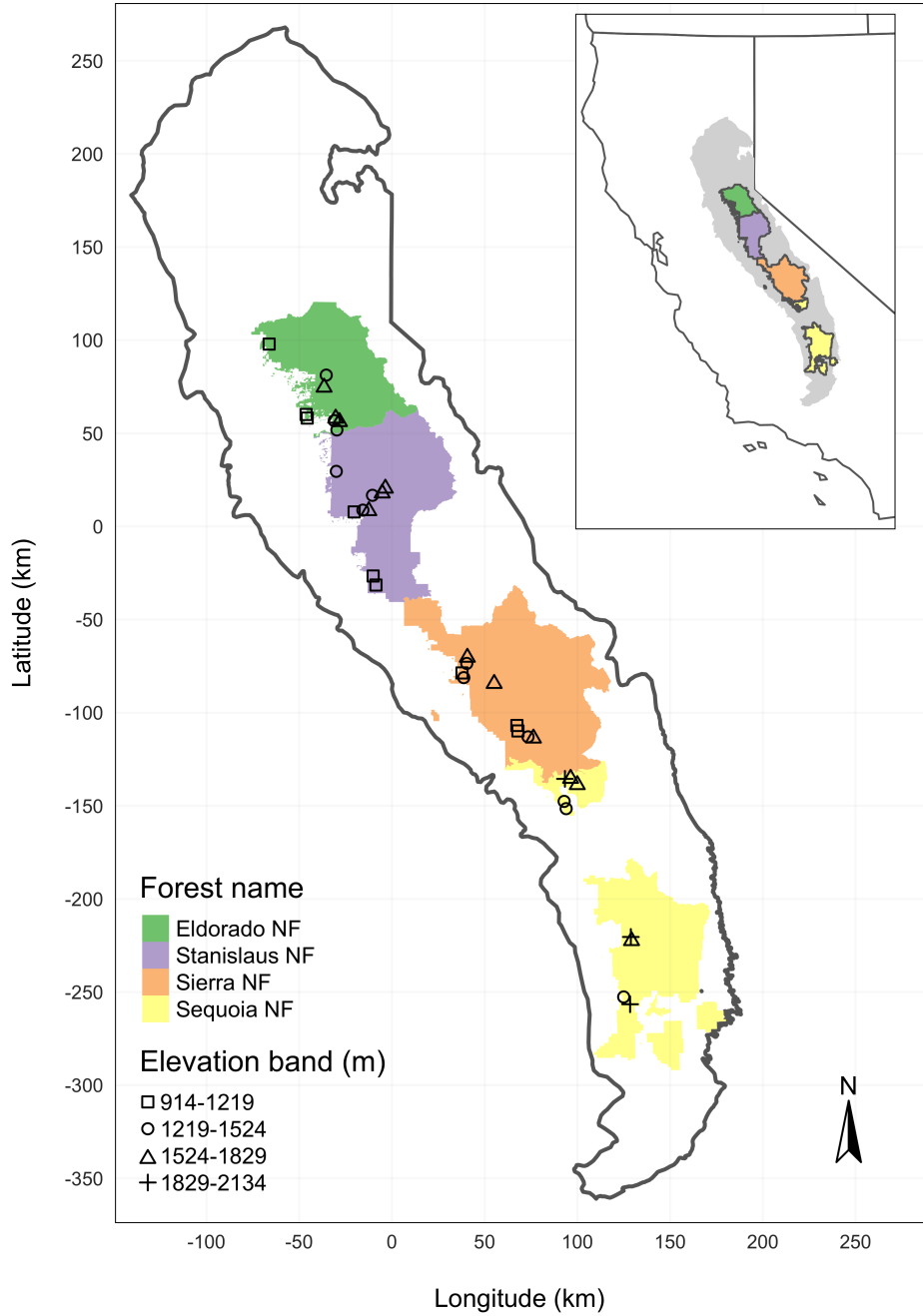


Figure 1: The network of field plots spanned a 350-km latitudinal gradient from the Eldorado National Forest in the north to the Sequoia National Forest in the south. Plots were stratified by three elevation bands in each forest, with the plots in the Sequoia National Forest (the southern-most National Forest) occupying elevation bands 305 m above the three bands in the other National Forests in order to capture a similar community composition.

154 Stanislaus, Sierra and Sequoia National Forests and were stratified by elevation (914-1219 m, 1219-1524  
155 m, 1524-1829 m above sea level). In the Sequoia National Forest, the southernmost National Forest in our  
156 study, plots were stratified with the lowest elevation band of 1219-1524 m and extended to an upper elevation  
157 band of 1829-2134 m to capture a more similar forest community composition as at the more northern  
158 National Forests. The sites have variable forest structure and plot locations were selected in areas with >35%  
159 ponderosa pine basal area and >10% ponderosa pine mortality. At each site, five 0.041-ha circular plots  
160 were installed along transects with 80 to 200m between plots. In the field, Fettig et al. (2019) mapped all  
161 stem locations relative to the center of each plot using azimuth/distance measurements. Tree identity to  
162 species, tree height, and diameter at breast height (DBH) were recorded if DBH was greater than 6.35cm.  
163 Year of mortality was estimated based on needle color and retention if it occurred prior to plot establishment,  
164 and was directly observed thereafter during annual site visits. A small section of bark (approximately 625  
165 cm<sup>2</sup>) on both north and south aspects was removed from dead trees to determine if bark beetle galleries  
166 were present. The shape, distribution, and orientation of galleries are commonly used to distinguish among  
167 bark beetle species (Fettig 2016). In some cases, deceased bark beetles were present beneath the bark to  
168 supplement identifications based on gallery formation. During the spring and early summer of 2018, all field  
169 plots were revisited to assess whether dead trees had fallen (Fettig et al. 2019).

170 In the typical life cycle of WPBs, females initiate host colonization by tunneling through the outer bark and  
171 into the phloem and outer xylem where they rupture resin canals.

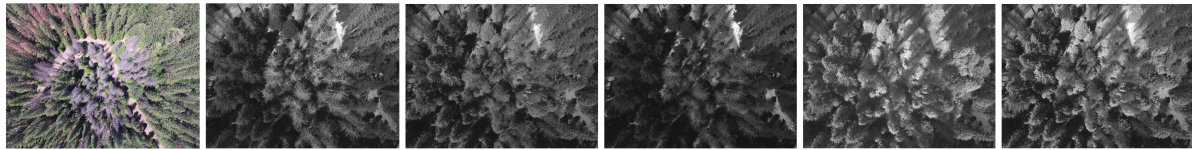
172 As a result, oleoresin exudes and collects on the bark surface, as is commonly observed with other bark beetle  
173 species. During the early stages of attack, females release an aggregation pheromone component which, in  
174 combination with host monoterpenes released from pitch tubes, is attractive to conspecifics (Bedard et al.  
175 1969). An antiaggregation pheromone component is produced during latter stages of host colonization by  
176 several pathways, and is thought to reduce intraspecific competition by altering adult behavior to minimize  
177 overcrowding of developing brood within the host (Byers and Wood 1980). Volatiles from several nonhosts  
178 sympatric with ponderosa pine have been demonstrated to inhibit attraction of WPB to its aggregation  
179 pheromones (Fettig et al. 2005, Shepherd et al. 2007). In California, WPB generally has 2-3 generations  
180 in a single year and can often out-compete other primary bark beetles such as the mountain pine beetle in  
181 ponderosa pines, especially in larger trees (Miller and Keen 1960).

## 182 **Aerial data collection and processing**

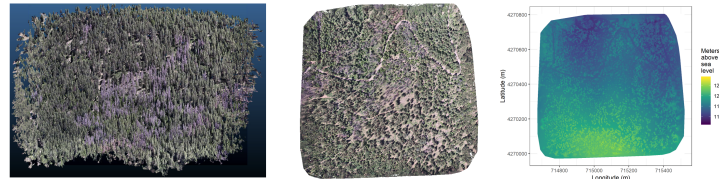
183 Nadir-facing imagery was captured using a gimbal-stabilized DJI Zenmuse X3 broad-band red/green/blue  
184 (RGB) camera (DJI 2015a) and a fixed-mounted Micasense Rededge3 multispectral camera with five narrow

bands (Micasense 2015) on a DJI Matrice 100 aircraft (DJI 2015b). Imagery was captured from both cameras along preprogrammed aerial transects over ~40 ha surrounding each of the 32 sites (each of these containing five field plots) and was processed in a series of steps to yield local forest structure and composition data suitable for our statistical analyses. All images were captured in 2018 during a 3-month period between early April and early July, and thus our work represents a postmortem investigation into the drivers of cumulative tree mortality. Following the call by Wyngaard et al. (2019), we establish “data product levels” to reflect the image processing pipeline from raw imagery (Level 0) to calibrated, fine-scale forest structure and composition information on regular grids (Level 4), with each new data level derived from levels below it. Here, we outline the steps in the processing and calibration pipeline visualized in Figure 2, and include additional details in the Supplemental Information.

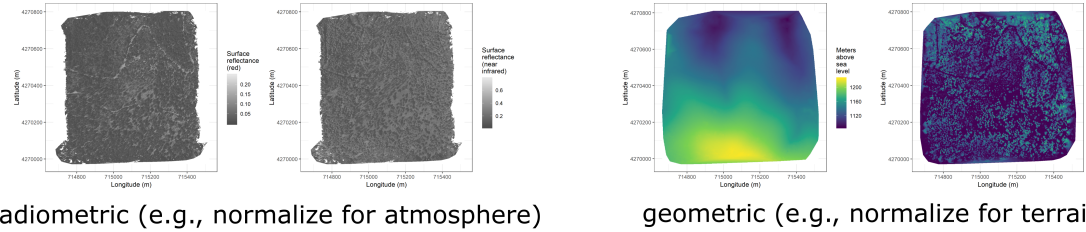
## Level 0: raw data from sensors



## Level 1: basic outputs from photogrammetric processing



## Level 2: corrected outputs from photogrammetric processing

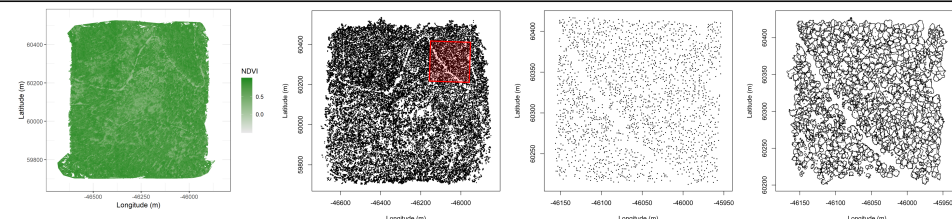


radiometric (e.g., normalize for atmosphere)

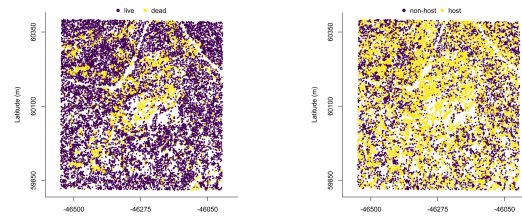
geometric (e.g., normalize for terrain)

## Level 3: domain-specific information extraction

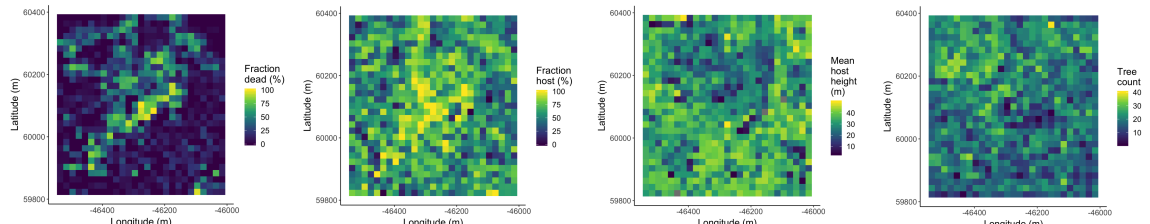
L3a  
spectral  
OR  
geometric



L3b  
spectral  
AND  
geometric



## Level 4: aggregations to regular grids



196 Figure 2. Schematic of the data processing workflow for a single site with each new data product level derived  
197 from data at lower levels.

198 Level 0 represents raw data from the sensors. From left to right: example broad-band RGB photo from  
199 DJI Zenmuse X3 camera, example blue photo from Rededge3 (centered on 475nm), example green photo  
200 from Rededge3 (centered on 560nm), example red photo from Rededge3 (centered on 668nm), example near  
201 infrared photo from Rededge3 (centered on 840nm), and example red edge photo from Rededge3 (centered on  
202 717nm).

203 Level 1 represents basic outputs from the photogrammetric workflow, in this case implemented with  
204 Pix4Dmapper. From left to right: a dense point cloud visualized in CloudCompare (<https://www.danielgm.net/cc/>), an orthophoto generated from the RGB camera, and a digital surface model representing the  
205 altitude above sea level (ground height + vegetation height) for every cell.

207 Level 2 represents outputs from photogrammetric processing that have been corrected radiometrically or  
208 geometrically. From left to right: a radiometrically-corrected surface reflectance map of the red narrow band  
209 from the Rededge3 camera, a radiometrically-corrected surface reflectance map of the near infrared narrow  
210 band from the Rededge3 camera, a rasterized version of the digital terrain model derived by a geometric  
211 correction of the dense point cloud, and a canopy height model derived by subtracting the terrain height  
212 from the digital surface model.

213 Level 3 represents domain-specific information extraction from Level 2 products and is divided into two  
214 sub-levels. Level 3a products are derived using only spectral or only geometric data. From left to right: a  
215 reflectance map of Normalized Difference Vegetation Index (NDVI; Rouse et al. 1973) derived using the red  
216 and near infrared Level 2 reflectance products, a map of points representing detected trees from the canopy  
217 height model with a red polygon highlighting the area presented in more detail for the next two images, a  
218 close-up of points representing detected trees, and a close-up of polygons representing segmented tree crowns.  
219 Level 3b products are derived using both spectral and geometric data. From left to right: a map of the point  
220 locations of detected trees that have been classified as alive or dead based on the pixel values within each  
221 segmented tree crown and a map of the point locations of detected trees classified to WPB host/non-host  
222 using the same spectral information. Note that our study relies on the generation of Level 3a products in  
223 order to combine them and create Level 3b products, but this need not be the case. For instance, deep  
224 learning/neural net methods may be able to use both the spectral and geometric information from Level 2  
225 simultaneously to locate and classify trees in a scene and directly generate Level 3b products without a need  
226 to first generate the Level 3a products shown in this schematic (Weinstein et al. 2019, dos Santos et al. 2019).

227 Level 4 represents aggregations of Level 3 products to regular grids which might better reflect the grain size  
228 of the data for which we have the best calibration and thus the most confidence or which might provide  
229 new information not possible at an individual-tree level (e.g., average distance between trees in a small  
230 neighborhood). From left to right: aggregation of live/dead classified trees as fraction of dead trees in a 20 x  
231 20-m cell, aggregation of host/non-host classified trees as fraction of hosts in a 20 x 20-m cell, aggregation of  
232 mean host height in a 20 x 20-m cell, and aggregation of tree count (including all species), in a 20 x 20-m  
233 cell. In our case, the 20 x 20-m aggregation produces a grid cell with an area of 400 m<sup>2</sup>, which most closely  
234 matches the 404-m<sup>2</sup> area of the ground-based vegetation plots whose data we used in an aggregated form to  
235 calibrate our derivation of Level 3 products.

#### 236 **Level 0: Raw data from sensors**

237 Raw data comprised approximately 1900 images per camera lens (one broad-band RGB lens and five narrow-  
238 band multispectral lenses) for each of the 32 sites (Figure 2; Level 0). Prior to the aerial survey, two strips of  
239 bright orange drop cloth (~100 x 15 cm) were positioned as an “X” over the permanent monuments marking  
240 the center of the 5 field plots from Fettig et al. (2019) (see Supplemental Information).

241 We preprogrammed north-south aerial transects using Map Pilot for DJI on iOS flight software (Drones-  
242 MadeEasy 2018) at an altitude of 120 m above ground level (with “ground” defined using a 1-arc-second  
243 digital elevation model (Farr et al. 2007)). The resulting ground sampling distance was approximately 5  
244 cm/px for the Zenmuse X3 RGB camera and approximately 8 cm/px for the Rededge3 multispectral camera.  
245 We used 91.6% image overlap (both forward and side) at the ground for the Zenmuse X3 RGB camera and  
246 83.9% overlap (forward and side) for the Rededge3 multispectral camera.

#### 247 **Level 1: Basic outputs from photogrammetric processing**

248 We used SfM photogrammetry implemented in Pix4Dmapper Cloud ([www.pix4d.com](http://www.pix4d.com)) to generate dense point  
249 clouds (Figure 2; Level 1, left), orthophotos (Figure 2; Level 1, center), and digital surface models (Figure 2;  
250 Level 1, right) for each field site (Frey et al. 2018). For 29 sites, we processed the Rededge3 multispectral  
251 imagery alone to generate these products. For three sites, we processed the RGB and the multispectral  
252 imagery together to enhance the point density of the dense point cloud. All SfM projects resulted in a single  
253 processing “block,” indicating that all images in the project were optimized and processed together. The  
254 dense point cloud represents x, y, and z coordinates as well as the color of millions of points per site. The  
255 orthophoto represents a radiometrically uncalibrated, top-down view of the survey site that preserves the  
256 relative x-y positions of objects in the scene. The digital surface model is a rasterized version of the dense

257 point cloud that shows the altitude above sea level for each pixel in the scene at the ground sampling distance  
258 of the camera that generated the Level 0 data.

259 **Level 2: Corrected outputs from photogrammetric processing**

260 **Radiometric corrections**

261 A radiometrically-corrected reflectance map (Figure 2; Level 2, left two figures; i.e., a corrected version of the  
262 Level 1 orthophoto) was generated using the Pix4D software by incorporating incoming light conditions for  
263 each narrow band of the Rededge3 camera (captured simultaneously with the Rededge3 camera using an  
264 integrated downwelling light sensor) as well as a pre-flight image of a calibration panel of known reflectance  
265 (see Supplemental Information for camera and calibration panel details).

266 **Geometric corrections**

267 We implemented a geometric correction to the Level 1 dense point cloud and digital surface model by  
268 normalizing these data for the terrain underneath the vegetation. We generated the digital terrain model  
269 representing the ground underneath the vegetation at 1-m resolution (Figure 2; Level 2, third image) by  
270 classifying each survey area’s dense point cloud into “ground” and “non-ground” points using a cloth simulation  
271 filter algorithm (Zhang et al. 2016) implemented in the `lidR` (Roussel et al. 2019) package and rasterizing  
272 the ground points using the `raster` package (Hijmans et al. 2019). We generated a canopy height model  
273 (Figure 2; Level 2, fourth image) by subtracting the digital terrain model from the digital surface model.

274 **Level 3: Domain-specific information extraction**

275 **Level 3a: Data derived from spectral OR geometric Level 2 product**

276 Using just the spectral information from the radiometrically-corrected reflectance maps, we calculated several  
277 vegetation indices including the normalized difference vegetation index (NDVI; Rouse et al. (1973); Figure  
278 2; Level 3a, first image), the normalized difference red edge (NDRE; Gitelson and Merzlyak (1994)), the  
279 red-green index (RGI; Coops et al. (2006)), the red edge chlorophyll index ( $CI_{red\ edge}$ ; Clevers and Gitelson  
280 (2013)), and the green chlorophyll index ( $CI_{green}$ ; Clevers and Gitelson (2013)).

Table 1: Algorithm name, number of parameter sets tested for each algorithm, and references.

| Algorithm | Parameter sets tested | Reference(s)  |
|-----------|-----------------------|---|
| li2012    | 131                   | Li et al. (2012); Jakubowski et al.<br>(2013); Shin et al. (2018) |

| Algorithm   | Parameter sets tested | Reference(s)          |
|-------------|-----------------------|-----------------------|
| lmfx        | 30                    | Roussel (2019)        |
| localMaxima | 6                     | Roussel et al. (2019) |
| multichm    | 1                     | Eysn et al. (2015)    |
| ptrees      | 3                     | Vega et al. (2014)    |
| vwf         | 3                     | Plowright (2018)      |
| watershed   | 3                     | Pau et al. (2010)     |

Using just the geometric information from the canopy height model or terrain-normalized dense point cloud, we generated maps of detected trees (Figure 2; Level 3a, second and third images) by testing a total of 7 automatic tree detection algorithms and a total of 177 parameter sets (Table 1). We used the field plot data to assess each tree detection algorithm/parameter set by converting the distance-from-center and azimuth measurements of the trees in the field plots to x-y positions relative to the field plot centers distinguishable in the Level 2 reflectance maps as the orange fabric X's that we laid out prior to each flight. In the reflectance maps, we located 110 out of 160 field plot centers while some plot centers were obscured due to dense interlocking tree crowns or because a plot center was located directly under a single tree crown. For each of the 110 field plots with identifiable plot centers— the “validation field plots”, we calculated 7 forest structure metrics using the ground data collected by Fettig et al. (2019): total number of trees, number of trees greater than 15 m in height, mean height of trees, 25<sup>th</sup> percentile tree height, 75<sup>th</sup> percentile tree height, mean distance to nearest tree neighbor, and mean distance to second nearest neighbor. For each tree detection algorithm and parameter set described above, we calculated the same set of 7 structure metrics within the footprint of the validation field plots. We calculated the Pearson’s correlation and root mean square error (RMSE) between the ground data and the aerial data for each of the 7 structure metrics for each of the 177 automatic tree detection algorithms/parameter sets. For each algorithm and parameter set, we calculated its performance relative to other algorithms as whether its Pearson’s correlation was within 5% of the highest Pearson’s correlation as well as whether its RMSE was within 5% of the lowest RMSE. We summed the number of forest structure metrics for which it reached these 5% thresholds for each algorithm/parameter set. For automatically detecting trees across the whole study, we selected the algorithm/parameter set that performed well across the most number of forest metrics (see Results).

We delineated individual tree crowns (Figure 2; Level 3a, fourth image) with a marker controlled watershed segmentation algorithm (Meyer and Beucher 1990) implemented in the **ForestTools** package (Plowright

304 2018) using the detected treetops as markers. If the automatic segmentation algorithm failed to generate  
305 a crown segment for a detected tree (e.g., often snags with a very small crown footprint), a circular crown  
306 was generated with a radius of 0.5 m. If the segmentation generated multiple polygons for a single detected  
307 tree, only the polygon containing the detected tree was retained. Because image overlap decreases near the  
308 edges of the overall flight path and reduces the quality of the SfM processing in those areas, we excluded  
309 segmented crowns within 35 m of the edge of the survey area. Given the narrower field of view of the Rededge3  
310 multispectral camera versus the X3 RGB camera whose optical parameters were used to define the ~40 ha  
311 survey area around each site, as well as the 35 m additional buffering, the survey area at each site was ~30  
312 ha (see Supplemental Information).

### 313 **Level 3b: Data derived from spectral AND geometric information**

314 We overlaid the segmented crowns on the reflectance maps from 20 sites spanning the latitudinal and elevation  
315 gradient in the study. Using QGIS (<https://qgis.org/en/site/>), we hand classified 564 trees as live/dead  
316 (Figure 3) and as one of 5 dominant species in the study area (ponderosa pine, *Pinus lambertiana*, *Abies*  
317 *concolor*, *Calocedrus decurrens*, or *Quercus kelloggii*) using the mapped ground data as a guide. Each tree was  
318 further classified as “host” for ponderosa pine or “non-host” for all other species (Fettig 2016). We extracted  
319 all the pixel values within each segmented crown polygon from the five, Level 2 orthorectified reflectance  
320 maps (one per narrow band on the Rededge3 camera) as well as from the five, Level 3a vegetation index  
321 maps using the *velox* package (Hunziker 2017). For each crown polygon, we calculated the mean value of  
322 the extracted Level 2 and Level 3a pixels and used them as ten independent variables in a five-fold cross  
323 validated boosted logistic regression model to predict whether the hand classified trees were alive or dead.  
324 For just the living trees, we similarly used all 10 mean reflectance values per crown polygon to predict tree  
325 species using a five-fold cross validated regularized discriminant analysis. The boosted logistic regression and  
326 regularized discriminant analysis were implemented using the *caret* package in R (Kuhn 2008). We used  
327 these models to classify all tree crowns in the data set as alive or dead (Figure 2; Level 3b, first image) as  
328 well as the species of living trees (Figure 2; Level 3b, second image). Finally, we estimated the basal area of  
329 each tree from their photogrammetry-derived height using species-specific simple linear regressions of the  
330 relationship between height and DBH as measured in the coincident field plots from Fettig et al. (2019).

### 331 **Level 4: Aggregations to regular grids**

332 We rasterized the forest structure and composition data at a spatial resolution similar to that of the field  
333 plots to better match the grain size at which we validated the automatic tree detection algorithms. In each  
334 raster cell, we calculated: number of dead trees, number of ponderosa pine trees, total number of trees, and

335 mean height of ponderosa pine trees. The values of these variables in each grid cell and derivatives from  
336 them were used for visualization and modeling. Here, we show the fraction of dead trees per cell (Figure 2;  
337 Level 4, first image), the fraction of host trees per cell (Figure 2; Level 4, second image), the mean height of  
338 ponderosa pine trees in each cell (Figure 2; Level 4, third image), and the total count of trees per cell (Figure  
339 2; Level 4, fourth image).

340 **Note on assumptions about dead trees**

341 For the purposes of this study, we assumed that all dead trees were ponderosa pine and thus hosts colonized  
342 by WPB. This is a reasonably good assumption for our study area; for example, Fettig et al. (2019) found  
343 that 73.4% of dead trees in their coincident field plots were ponderosa pine. Mortality was concentrated in  
344 the larger-diameter classes and attributed primarily to WPB (see Figure 5 of Fettig et al. 2019). The species  
345 contributing to the next highest proportion of dead trees was incense cedar which represented 18.72% of the  
346 dead trees in the field plots. While the detected mortality is most likely to be ponderosa pine killed by WPB,  
347 it is critical to interpret our results with these limitations in mind.

348 **Environmental data**

349 We used CWD (Stephenson 1998) from the 1981-2010 mean value of the basin characterization model (Flint  
350 et al. 2013) as an integrated measure of historic temperature and moisture conditions for each of the 32 sites.  
351 Higher values of CWD correspond to historically hotter, drier conditions and lower values correspond to  
352 historically cooler, wetter conditions. CWD has been shown to correlate well with broad patterns of tree  
353 mortality in the Sierra Nevada (Young et al. 2017) as well as bark beetle-induced tree mortality (Millar  
354 et al. 2012). The forests along the entire CWD gradient used in this study experienced exceptional hot  
355 drought between 2012 to 2015 with a severity of at least a 1,200-year event, and perhaps more severe than  
356 a 10,000-year event (Griffin and Anchukaitis 2014, Robeson 2015). We converted the CWD value for each  
357 site into a z-score representing that site's deviation from the mean CWD across the climatic range of Sierra  
358 Nevada ponderosa pine as determined from 179 herbarium records described in Baldwin et al. (2017). Thus,  
359 a CWD z-score of 1 would indicate that the CWD at that site is one standard deviation hotter/drier than  
360 the mean CWD across all geolocated herbarium records for ponderosa pine in the Sierra Nevada.

361 **Statistical model**

362 We used a generalized linear model with a zero-inflated binomial response and a logit link to predict the  
363 probability of ponderosa pine mortality within each 20 x 20-m cell using the total number of ponderosa  
364 pine trees in each cell as the number of trials, and the number of dead trees in each cell as the number of

365 “successes”. As covariates, we used the proportion of trees that are WPB hosts (i.e., ponderosa pine) in each  
 366 cell, the mean height of ponderosa pine trees in each cell, the count of trees of all species (overall density) in  
 367 each cell, and the site-level CWD using Eq. 1. Note that the two-way interaction between the overall density  
 368 and the proportion of trees that are hosts is directly proportional to the number of ponderosa pine trees in  
 369 the cell. We centered and scaled all predictor values, and used weakly-regularizing default priors from the  
 370 `brms` package (Bürkner 2017). To measure and account for spatial autocorrelation underlying ponderosa pine  
 371 mortality, we subsampled the data at each site to a random selection of 200, 20 x 20-m cells representing  
 372 approximately 27.5% of the surveyed area. Additionally with these subsampled data, we included a separate  
 373 exact Gaussian process term per site of the noncentered/nonscaled interaction between the x- and y-position  
 374 of each cell using the `gp()` function in the `brms` package (Bürkner 2017). The Gaussian process estimates the  
 375 spatial covariance in the response variable (log-odds of ponderosa pine mortality) jointly with the effects of  
 376 the other covariates.

$$\begin{aligned}
 y_{i,j} &\sim \begin{cases} 0, & p \\ Binom(n_i, \pi_i), & 1 - p \end{cases} \\
 logit(\pi_i) &= \beta_0 + \\
 &\beta_1 X_{cwd,j} + \beta_2 X_{propHost,i} + \beta_3 X_{PipoHeight,i} + \\
 &\beta_4 X_{overallDensity,i} + \beta_5 X_{overallBA,i} + \\
 &\beta_6 X_{cwd,j} X_{PipoHeight,i} + \beta_7 X_{cwd,j} X_{propHost,i} + \\
 &\beta_8 X_{cwd,j} X_{overallDensity,i} + \beta_9 X_{cwd,j} X_{overallBA,i} + \\
 &\beta_{10} X_{propHost,i} X_{PipoHeight,i} + \beta_{11} X_{propHost,i} X_{overallDensity,i} + \\
 &\beta_{12} X_{cwd,j} X_{propHost,i} X_{PipoHeight,i} + \\
 &\mathcal{GP}_j(x_i, y_i)
 \end{aligned}$$

377 Where  $y_i$  is the number of dead trees in cell  $i$ ,  $n_i$  is the sum of the dead trees (assumed to be ponderosa pine)  
 378 and live ponderosa pine trees in cell  $i$ ,  $\pi_i$  is the probability of ponderosa pine tree mortality in cell  $i$ ,  $p$  is the  
 379 probability of there being zero dead trees in a cell arising as a result of an independent, unmodeled process,  
 380  $X_{cwd,j}$  is the z-score of CWD for site  $j$ ,  $X_{propHost,i}$  is the scaled proportion of trees that are ponderosa pine  
 381 in cell  $i$ ,  $X_{PipoHeight,i}$  is the scaled mean height of ponderosa pine trees in cell  $i$ ,  $X_{overallDensity,i}$  is the scaled  
 382 density of all trees in cell  $i$ ,  $X_{overallBA,i}$  is the scaled basal area of all trees in cell  $i$ ,  $x_i$  and  $y_i$  are the x- and  
 383 y- coordinates of the centroid of the cell in an EPSG3310 coordinate reference system, and  $\mathcal{GP}_j$  represents

384 the exact Gaussian process describing the spatial covariance between cells at site  $j$ .

385 We fit this model using the `brms` package (Bürkner 2017) which implements the No U-Turn Sampler extension  
386 to the Hamiltonian Monte Carlo algorithm (Hoffman and Gelman 2014) in the Stan programming language  
387 (Carpenter et al. 2017). We used 4 chains with 4000 iterations each (2000 warmup, 2000 samples), and  
388 confirmed chain convergence by ensuring all `Rhat` values were less than 1.1 (Brooks and Gelman 1998) and  
389 that the bulk and tail effective sample sizes (ESS) for each estimated parameter were greater than 100 times  
390 the number of chains (i.e., greater than 400 in our case). We used posterior predictive checks to visually  
391 confirm model performance by overlaying the density curves of the predicted number of dead trees per cell  
392 over the observed number (Gabry et al. 2019). For the posterior predictive checks, we used 50 random  
393 samples from the model fit to generate 50 density curves and ensured curves were centered on the observed  
394 distribution, paying special attention to model performance at capturing counts of zero.

### 395 Data availability

396 All data are available via the Open Science Framework (DOI available upon publication).

### 397 Code availability

398 Statistical analyses were performed using the `brms` packages. With the exception of the SfM software  
399 (Pix4Dmapper Cloud) and the GIS software QGIS, all data carpentry and analyses were performed using R  
400 (R Core Team 2018). All code used to generate the results from this study are available via the Open Science  
401 Framework.

## 402 Results

### 403 Tree detection algorithm performance

404 We found that the experimental `lmfx` algorithm with parameter values of `dist2d = 1` and `ws = 2.5` (Roussel  
405 et al. 2019) performed the best across 7 measures of forest structure as measured by Pearson's correlation  
406 with ground data (Table 2).

Table 2: Correlation and differences between the best performing tree detection algorithm (lmfx with dist2d = 1 and ws = 2.5) and the ground data. An asterisk next to the correlation or RMSE indicates that this value was within 5% of the value of the best-performing algorithm/parameter set. Ground mean represents the mean value of the forest metric across the 110 field plots that were visible from the sUAS-derived imagery. The median error is calculated as the median of the differences between the air and ground values for the 110 visible plots. Thus, a positive number indicates an overestimate by the sUAS workflow and a negative number indicates an underestimate.

| Forest structure metric                 | Ground mean | Correlation with ground | RMSE   | Median error |
|---|-------------|-------------------------|--------|--------------|
| total tree count                        | 19          | 0.67*                   | 8.68*  | 2            |
| count of trees > 15 m                   | 9.9         | 0.43                    | 7.38   | 0            |
| distance to 1st neighbor (m)            | 2.8         | 0.55*                   | 1.16*  | 0.26         |
| distance to 2nd neighbor (m)            | 4.3         | 0.61*                   | 1.70*  | 0.12         |
| height (m); 25 <sup>th</sup> percentile | 12          | 0.16                    | 8.46   | -1.2         |
| height (m); mean                        | 18          | 0.29                    | 7.81*  | -2.3         |
| height (m); 75 <sup>th</sup> percentile | 25          | 0.35                    | 10.33* | -4           |

407 **Classification accuracy for live/dead and host/non-host**

408 The accuracy of live/dead classification on a withheld test dataset was 96.4%. The accuracy of species  
 409 classification on a withheld testing dataset was 64.1%. The accuracy of WPB host/non-WPB-host (i.e.,  
 410 ponderosa pine versus other tree species) on a withheld testing dataset was 71.8%.

411 **Site summary based on best tree detection algorithm and classification**

412 Across all study sites, we detected, segmented, and classified 452,413 trees. Of these trees, we classified  
 413 118,879 as dead (26.3% mortality). Estimated site-level tree mortality ranged from 6.8% to 53.6%. See  
 414 Supplemental Information for site summaries and comparisons to site-level mortality measured from field  
 415 data.

416 **Effect of local structure and regional climate on tree mortality attributed to western pine  
 417 beetle**

418 Site-level CWD exerted a positive, but relatively weak, main effect on the probability of ponderosa mortality  
 419 (effect size: 0.16; 95% CI: [0.03, 0.30]; Figure 4). We found a positive main effect of proportion of host trees  
 420 per cell (effect size: 0.76; 95% CI: [0.70, 0.82]), with a greater proportion of host trees (i.e., ponderosa pine)  
 421 in a cell increasing the probability of ponderosa pine mortality. We detected no effect of overall tree density

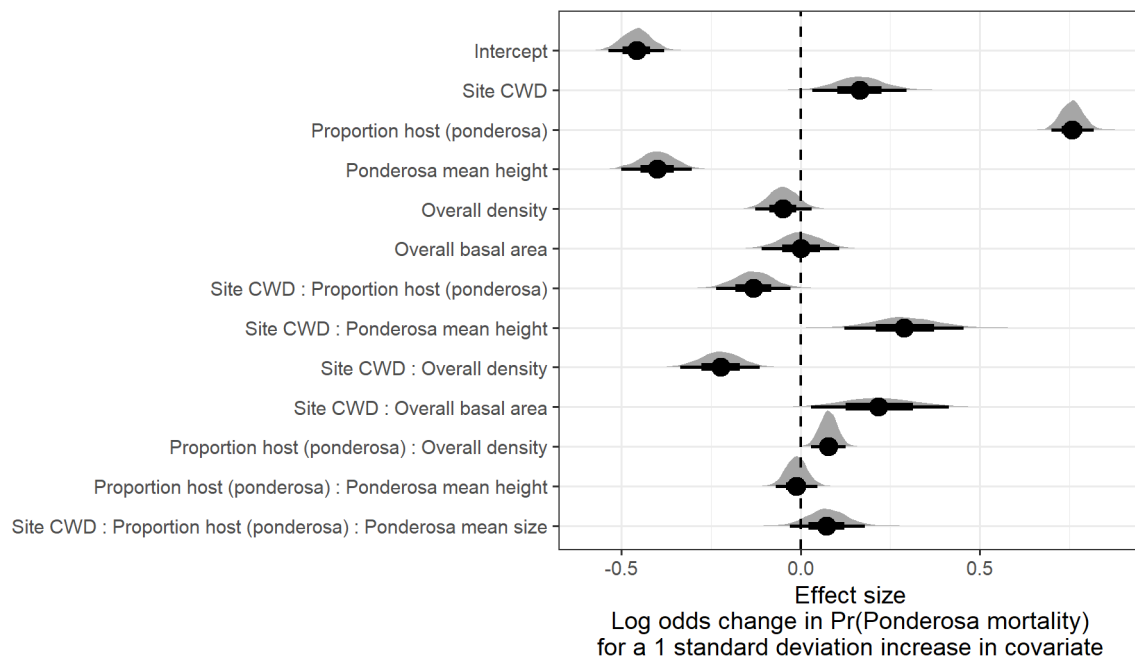


Figure 4: Posterior distributions of effect size from zero-inflated binomial model predicting the probability of ponderosa pine mortality in a 20 x 20-m cell given forest structure characteristics and site-level climatic water deficit (CWD). The gray filled area for each model covariate represents the probability density of the posterior distribution, the point underneath each density curve represents the median of the estimate, the bold interval surrounding the point estimate represents the 66% credible interval, and the thin interval surrounding the point estimate represents the 95% credible interval.

422 nor overall basal area (i.e., including both ponderosa pine and non-host species; tree density effect size: -0.05;  
423 95% CI: [-0.13, 0.03]; basal area effect size: 0.00; 95% CI: [-0.11, 0.11]).

424 We found a positive two-way interaction between the overall tree density per cell and the proportion of trees  
425 that were hosts, which is equivalent to a positive effect of the density of host trees (effect size: 0.08; 95% CI:  
426 [0.03, 0.13]; Figure 4).

427 We found a negative effect of mean height of ponderosa pine on the probability of ponderosa mortality,  
428 suggesting that WPB attacked smaller trees, on average (effect size: -0.40; 95% CI: [-0.50, -0.30]). However,  
429 there was a positive interaction between CWD and ponderosa pine mean height, such that larger trees were  
430 more likely to increase the local probability of ponderosa mortality in hotter, drier sites (effect size: 0.29;  
431 95% CI: [0.12, 0.46]; Figure 5).

432 We found weakly negative effects of the site-level CWD interactions with both the proportion of host trees  
433 and overall tree density (CWD/proportion host interaction effect size: -0.13; 95% CI: [-0.23, -0.03]; Figure 4;  
434 CWD/overall tree density interaction effect size: -0.22; 95% CI: [-0.34, -0.11]; Figure 4; Figure 5). We found  
435 a positive effect of the interaction between CWD and total basal area (effect size: 0.22; 95% CI: [0.03, 0.42];  
436 Figure 4; Figure 5).

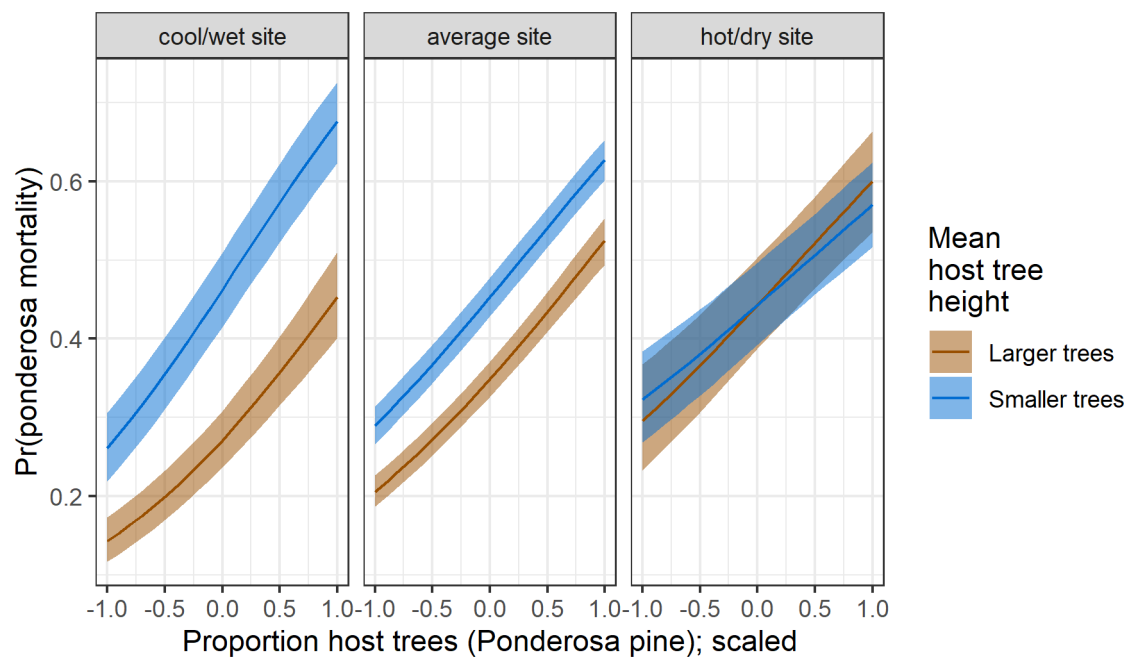


Figure 5: Line version of model results with 95% credible intervals showing primary influence of ponderosa pine structure on the probability of ponderosa pine mortality, and the interaction across climatic water deficit. The ‘larger trees’ line represents the mean height of ponderosa pine 0.7 standard deviations above the mean (approximately 24.1 m), and the ‘smaller trees’ line represents the mean height of ponderosa pine 0.7 standard deviations below the mean (approximately 12.1 m).

437 **Discussion**

438 This study represents a novel use of drones to refine our understanding of the patterns of tree mortality  
439 following the 2012 to 2015 California hot drought and its aftermath. By simultaneously measuring the effects  
440 of local forest structure and composition with broad-scale environmental gradients, we were able to better  
441 characterize the disturbance amplifying effect of a tree-killing insect, the WPB, compared to using correlates  
442 of tree stress alone.

443 **Weak positive main effect of CWD**

444 We found only a relatively weak positive effect of site-level CWD on ponderosa pine mortality rate. To that  
445 end, we did not measure tree water stress at an individual tree level as in other recent work (Stephenson et  
446 al. 2019), and instead treated CWD as a general indicator of tree stress following results of coarser-scale  
447 studies (e.g., Young et al. 2017), which may have contributed to our failure to detect a stronger CWD effect.  
448 When measured at a fine scale, even if not at an individual tree level, progressive canopy water loss can be  
449 a good indicator of tree water stress and increased vulnerability to mortality from drought or bark beetles  
450 (Brodrick and Asner 2017). Our entire study area experienced exceptional hot drought between 2012 and  
451 2015 (Griffin and Anchukaitis 2014, Robeson 2015) and the variation of mortality explained by a main effect  
452 of CWD may be dampened when most trees are experiencing a high degree of water stress (Floyd et al. 2009,  
453 Fettig et al. 2019). Importantly, using a 30-year historic average of CWD as a site-level indicator of tree  
454 stress doesn't allow us to disentangle whether water availability was lower in an absolute sense during the  
455 drought or whether increasing tree vulnerability to bark beetles was driven by chronic water stress at these  
456 historically hotter/drier sites (McDowell et al. 2008).

457 **Positive effect of host density and a negative effect of overall density**

458 A number of mechanisms associated with the relative abundance of species in a local area might underlie the  
459 strong effect of host proportion on the probability of host tree mortality. Frequency-dependent herbivory—  
460 whereby mixed-species forests experience less herbivory compared to monocultures (as an extreme example)—  
461 is common, especially for oligophagous insect species (Jactel and Brockerhoff 2007). Nonhost volatiles reduce  
462 attraction of several species of bark beetles to their aggregation pheromones (Seybold et al. 2018), including  
463 WPB (Fettig et al. 2005). Combinations of nonhost volatiles and an antiaggregation pheromone have been  
464 used successfully to reduce levels of tree mortality attributed to WPB in California (e.g., Fettig et al. 2008,  
465 2012). Hayes et al. (2009) and Fettig et al. (2019) found that measures of host availability explained less  
466 variation in mortality than measures of overall tree density. Those conclusions, however, were based on a

467 response variable of “total number of dead host trees,” rather than the number of dead host trees conditional  
468 on the total number of host trees as in our study (i.e., a binomial response).

469 The negative relationship between overall tree density and the probability of ponderosa pine mortality  
470 corroborates findings of coincident ground plots (Fettig et al. 2019, in their analysis using proportion of trees  
471 killed as a response) and other work during the same hot drought (Restaino et al. 2019). In the absence of  
472 management, forest structure is largely a product of climate and, with increasing importance at finer spatial  
473 scales, topographic conditions (Fricker et al. 2019). Denser forest patches in our study may indicate greater  
474 local water availability, more favorable conditions for tree growth and survivorship, and increased resistance  
475 to beetle-induced tree mortality (Ma et al. 2010, Restaino et al. 2019, Fricker et al. 2019). The negative  
476 two-way interaction between site CWD and overall density that amplifies the negative overall density effect  
477 in hotter, drier sites (effect size: -0.22; 95% CI: [-0.34, -0.11]) supports this explanation if greater local tree  
478 density implies especially favorable growing conditions (and locally resistant trees) when denser patches are  
479 found in hot, dry sites.

480 The positive relationship between host density and susceptibility to colonization by bark beetles has been so  
481 well-documented at the experimental plot level (e.g., Raffa and Berryman 1987, Oliver 1995) that lowering  
482 stand densities through selective harvest of hosts is commonly recommended for reducing future levels of tree  
483 mortality attributed to bark beetles (Fettig and Hilszczański 2015), including WPB (Fettig 2016). Greater  
484 host density shortens the flight distance required for WPB to disperse to new hosts, which likely facilitates  
485 bark beetle spread, however we calibrated our aerial tree detection to ~400 m<sup>2</sup> areas rather than to individual  
486 tree locations, so our data are insufficient to address these relationships. Increased density of ponderosa pine,  
487 specifically, may disproportionately increase the competitive environment for host trees (and thus increase  
488 their susceptibility to WPB colonization) if intraspecific competition amongst ponderosa pine trees is stronger  
489 than interspecific competition as would be predicted with coexistence theory (Chesson 2000). Finally, greater  
490 host densities increase the frequency that searching WPB land on hosts, rather than nonhosts, thus reducing  
491 the amount of energy expended during host finding and selection as well as the time that searching WPB  
492 spend exposed to a variety of predators outside the host tree.

#### 493 Positive interaction effect of CWD and basal area

494 While overall tree density is likely an indicator of favorable microsites in fire-suppressed forests, overall basal  
495 area is a better indicator of the local competitive environment especially in water-limited forests (Ma et al.  
496 2010, Fricker et al. 2019). While we found no main effect of overall basal area on the probability of ponderosa  
497 mortality, we did detect a clear interaction between site-level CWD and basal area such that mortality rates

498 of ponderosa pine in hotter, drier sites were greater when local overall basal area was high. This is a similar  
499 interaction as found by Young et al. (2017), and we perhaps did not detect a similar main effect of basal  
500 area as Young et al. (2017) because we partitioned this overall effect into the influence of finer-scale forest  
501 structure and composition (e.g., number of host trees).

502 **Negative main effect of host tree mean size, but strong positive interaction with site CWD**

503 The negative main effect of host tree mean size was surprising, and appears to contradict long-standing  
504 wisdom on the dynamics of WPB in the Sierra Nevada. WPB exhibit a preference for trees 50.8 to 76.2  
505 cm DBH (Person 1928, 1931), and a positive relationship between host tree size and levels of tree mortality  
506 attributed to WPB was reported by Fettig et al. (2019) in the coincident field plots as well as in other  
507 recent studies (Restaino et al. 2019, Stephenson et al. 2019, Pile et al. 2019). Indeed, Fettig et al. (2019)  
508 attributed no mortality to WPB in ponderosa pine trees <10.0 cm DBH and found no tree size/mortality  
509 relationship for incense cedar or white fir in the coincident field plots. These species represent 22.3% of the  
510 total tree mortality observed in their study, yet in our study all dead trees were classified as ponderosa pine  
511 (see Methods) which could dampen the positive effect of tree size on tree mortality. Larger trees are more  
512 nutritious and are therefore ideal targets if local bark beetle density is high enough to successfully initiate  
513 mass attack and overwhelm tree defenses, as can occur when many trees are under severe water stress (Bentz  
514 et al. 2010, Boone et al. 2011, Kolb et al. 2016). In the recent hot drought, we expected that most trees  
515 would be under severe water stress, setting the stage for increasing beetle density, successful mass attacks,  
516 and targeting of larger trees. A possible explanation for our finding counter to this expectation is that our  
517 observations represent the cumulative mortality of trees during a multi-year drought event and its aftermath.  
518 Lower host tree mean size led to a greater probability of host mortality earlier in this drought (Pile et al.  
519 2019, Stovall et al. 2019) and that signal might have persisted even as mortality continued to accumulate  
520 driven by other factors. Another explanation may be that our extensive sampling design better captured the  
521 contagious process by which bark beetles colonize smaller, suboptimal trees in the vicinity of the larger, more  
522 desirable trees that are the focus of initial attack (e.g., Klein et al. 1978). If larger, desirable trees tend to  
523 be associated with a greater local density of smaller trees that are also colonized in this contagious process,  
524 then we might observe a negative relationship between tree size and ponderosa mortality rates. Finally, tree  
525 growth rates may be a better predictor of susceptibility to WPB colonization than tree size per se, with  
526 slower-growing trees being most vulnerable (Miller and Keen 1960). While slow-growing trees are often also  
527 the largest trees, this may not be the case for our study sites especially given the legacy of fire suppression  
528 in the Sierra Nevada and its effect of perturbing forest structure far outside its natural range of variation  
529 (Safford and Stevens 2017).

530 In hot, dry sites, larger average host size increased the probability of host mortality while smaller host sizes  
531 increased the probability of host mortality in cooler, wetter sites. Notably, a similar pattern was shown  
532 by Stovall et al. (2019) with a strong positive tree height/mortality relationship in areas with the greatest  
533 vapor pressure deficit and no tree height/mortality relationship in areas with the lowest vapor pressure  
534 deficit. Stovall et al. (2019) did not observe that this environmental dependence extended to a negative tree  
535 height/mortality relationship (as we did) even at the lowest extremes of their vapor pressure deficit gradient,  
536 perhaps because their entire study took place in the southern Sierra Nevada which represents a hotter, drier  
537 portion of the more spatially extensive results we present here. Our work suggests that the WPB was cueing  
538 into different aspects of forest structure across an environmental gradient in a spatial context in a parallel  
539 manner to the temporal context noted by Stovall et al. (2019) and Pile et al. (2019), who observed that  
540 mortality was increasingly driven by larger trees as the hot drought proceeded and became more severe.

541 All of our sites were considered in an “epidemic” population phase for WPB (>5 trees killed per ha; see  
542 Supplemental Information; Miller and Keen 1960, Hayes et al. 2009), but our results challenge the notion  
543 that outbreak behavior by the WPB and subsequent tree mortality is always driven by greater tree size.  
544 Despite a strong tree size/mortality relationship in coincident ground plots across our study area (Fettig et al.  
545 2019), our results from surveying the broader context surrounding those ground plots reveals different effects  
546 of host tree size depending on CWD. Thus, it is possible that the massive tree mortality in hotter/drier  
547 Sierra Nevada forests (lower latitudes and elevations; Asner et al. 2016, Young et al. 2017) during the 2012  
548 to 2015 hot drought arose as a synergistic alignment of environmental conditions and local forest structure  
549 that allowed WPB to successfully colonize large trees, rapidly increase in population size, and expand. The  
550 unexpectedly low mortality in cooler/wetter Sierra Nevada forests compared to model predictions based on  
551 coarser-scale forest structure data (Young et al. 2017) may result from a different WPB response to local  
552 forest structure due to a lack of an alignment with favorable climate conditions.

## 553 **Limitations and future directions**

554 We have demonstrated that drones can be effective means of collecting forest data at multiple, vastly different  
555 spatial scales to investigate a single, multi-scale phenomenon– from meters in between trees, to hundreds of  
556 meters of elevation, to hundreds of thousands of meters of latitude. Some limitations remain, but can be  
557 overcome with further refinements in the use of this tool for forest ecology. Most of these limitations arise  
558 from tree detection and classification uncertainty, making it imperative to work with field data for calibration  
559 and uncertainty reporting.

560 The greatest limitation in our study arising from classification uncertainty is in the assumption that all dead

561 trees were ponderosa pine, which we estimate from coincident field plots is true approximately 73.4% of  
562 the time. Because the forest structure factors influencing the likelihood of individual tree mortality during  
563 the hot drought depended on tree species (Stephenson et al. 2019), we cannot rule out that some of the  
564 ponderosa pine mortality relationships to forest structure that we observed may be partially explained by  
565 those relationships in other species that were misclassified as ponderosa pine using our methods. However,  
566 the overall community composition across our study area was similar (Fettig et al. 2019) and we are able to  
567 reproduce similar forest structure/mortality patterns in drone-derived data when restricting the scope of  
568 analysis to only trees detected in the footprints of the coincident field plots, but with dramatically different  
569 patterns observed when including data from the forest surrounding the coincident field plots (see Supplemental  
570 information). Thus, we remain confident that the patterns we observed were driven primarily by the dynamic  
571 between WPB and ponderosa pine. While spectral information of foliage could help classify living trees to  
572 species, the species of standing dead trees were not spectrally distinct. This challenge of classifying standing  
573 dead trees to species implies that a conifer forest system with less bark beetle and tree host diversity, such  
574 as mountain pine beetle outbreaks in monocultures of lodgepole pine in the Intermountain West, should be  
575 particularly amenable to the methods presented here even with minimal further refinement because dead  
576 trees will almost certainly belong to a single species and have succumbed to colonization by a single bark  
577 beetle species.

578 Some uncertainty surrounded our ability to detect trees using the geometry of the dense point clouds derived  
579 with SfM. The horizontal accuracy of the tree detection was better than the vertical accuracy, which may  
580 result from a more significant error contribution by the field-based calculations of tree height compared to  
581 tree position relative to plot center (Table 2). Both the horizontal and vertical accuracy would likely improve  
582 with better SfM point clouds, which can be enhanced with greater overlap between images (Frey et al. 2018)  
583 or with oblique (i.e., off-nadir) imagery (James and Robson 2014). Frey et al. (2018) found that 95% overlap  
584 was preferable for generating dense point clouds in forested areas, and James and Robson (2014) reduced  
585 dense point cloud errors using imagery taken at 30 degrees off-nadir. We only achieved 91.6% overlap with  
586 the X3 RGB camera and 83.9% overlap with the multispectral camera, and all imagery was nadir-facing.  
587 While our live/dead classification was fairly accurate (96.4% on a withheld dataset), our species classifier  
588 would likely benefit from better crown segmentation because the pixel-level reflectance values within each  
589 crown are averaged to characterize the “spectral signature” of each tree. With better delineation of each  
590 tree crown, the mean value of pixels within each tree crown will likely be more representative of that tree’s  
591 spectral signature. Better crown segmentation might most readily be achieved through greater overlap in  
592 imagery. We anticipate that computer vision and deep learning will prove helpful in overcoming some of

593 these detection and classification challenges (Gray et al. 2019).

594 Finally, we note our study is constrained by using the probability of ponderosa mortality as our key response  
595 variable. This measure is well-suited to understanding the dynamics between WPB colonization behavior and  
596 host tree susceptibility, but may not capture impacts on the forest ecosystem and its services as well as a  
597 measure of biomass reduction such as tree basal area.

## 598 **Conclusions**

599 Climate change adaptation strategies emphasize management action that considers whole-ecosystem responses  
600 to inevitable change (Millar et al. 2007), which requires a macroecological understanding of how phenomena at  
601 multiple scales can interact. Tree vulnerability to environmental stressors presents only a partial explanation  
602 for tree mortality patterns during hot droughts, especially when bark beetles are present. We've shown that  
603 drones can be a valuable tool for investigating multi-scalar phenomena, such as how local forest structure  
604 combines with environmental conditions to shape forest insect disturbance. Understanding the conditions  
605 that drive dry western U.S. forest responses to disturbances such as bark beetle outbreaks will be vital for  
606 predicting outcomes from increasing disturbance frequency and intensity exacerbated by climate change  
607 (Vose et al. 2018). Our study suggests that outcomes will depend on interactions between local forest  
608 structure and broad-scale environmental gradients, with the potential for cross-scale interactions to enhance  
609 our understanding of forest insect dynamics.

610 **References**

- 611 Anderegg, W. R. L., J. A. Hicke, R. A. Fisher, C. D. Allen, J. Aukema, B. Bentz, S. Hood, J. W. Lichstein,  
612 A. K. Macalady, N. McDowell, Y. Pan, K. Raffa, A. Sala, J. D. Shaw, N. L. Stephenson, C. Tague, and  
613 M. Zeppel. 2015. Tree mortality from drought, insects, and their interactions in a changing climate. *New*  
614 *Phytologist* 208:674–683.
- 615 Asner, G. P., P. G. Brodrick, C. B. Anderson, N. Vaughn, D. E. Knapp, and R. E. Martin. 2016. Progressive  
616 forest canopy water loss during the 2012–2015 California drought. *Proceedings of the National Academy of*  
617 *Sciences* 113:E249–E255.
- 618 Baldwin, B. G., A. H. Thornhill, W. A. Freyman, D. D. Ackerly, M. M. Kling, N. Morueta-Holme, and B. D.  
619 Mishler. 2017. Species richness and endemism in the native flora of California. *American Journal of Botany*  
620 104:487–501.
- 621 Bedard, W. D., P. E. Tilden, D. L. Wood, R. M. Silverstein, R. G. Brownlee, and J. O. Rodin. 1969.  
622 Western pine beetle: Field response to its sex pheromone and a synergistic host terpene, myrcene. *Science*  
623 164:1284–1285.
- 624 Bentz, B. J., J. Régnière, C. J. Fettig, E. M. Hansen, J. L. Hayes, J. A. Hicke, R. G. Kelsey, J. F. Negrón,  
625 and S. J. Seybold. 2010. Climate change and bark beetles of the western United States and Canada: Direct  
626 and indirect effects. *BioScience* 60:602–613.
- 627 Berryman, A. A. 1982. Population dynamics of bark beetles. Pages 264–314 in *Bark Beetles in North*  
628 *American Conifers: A System for the Study of Evolutionary Biology*.
- 629 Boone, C. K., B. H. Aukema, J. Bohlmann, A. L. Carroll, and K. F. Raffa. 2011. Efficacy of tree defense  
630 physiology varies with bark beetle population density: A basis for positive feedback in eruptive species.  
631 *Canadian Journal of Forest Research* 41:1174–1188.
- 632 Brodrick, P. G., and G. P. Asner. 2017. Remotely sensed predictors of conifer tree mortality during severe  
633 drought. *Environmental Research Letters* 12:115013.
- 634 Brooks, S. P., and A. Gelman. 1998. General methods for monitoring convergence of iterative simulations.  
635 *Journal of Computational and Graphical Statistics* 7:434.
- 636 Bürkner, P.-C. 2017. **brms**: An *R* package for bayesian multilevel models using *Stan*. *Journal of Statistical*  
637 *Software* 80:1–28.
- 638 Byers, J. A., and D. L. Wood. 1980. Interspecific inhibition of the response of the bark beetles, *Dendroctonus*

- 639 *brevicomis* and *Ips paraconfusus*, to their pheromones in the field. Journal of Chemical Ecology 6:149–164.
- 640 Carpenter, B., A. Gelman, M. D. Hoffman, D. Lee, B. Goodrich, M. Betancourt, M. Brubaker, J. Guo, P. Li,  
641 and A. Riddell. 2017. Stan: A Probabilistic Programming Language. Journal of Statistical Software 76:1–32.
- 642 Chesson, P. 2000. Mechanisms of maintenance of species diversity. Annual Review of Ecology and Systematics  
643 31:343–366.
- 644 Chubaty, A. M., B. D. Roitberg, and C. Li. 2009. A dynamic host selection model for mountain pine beetle,  
645 *Dendroctonus ponderosae* Hopkins. Ecological Modelling 220:1241–1250.
- 646 Clevers, J., and A. Gitelson. 2013. Remote estimation of crop and grass chlorophyll and nitrogen content using  
647 red-edge bands on Sentinel-2 and -3. International Journal of Applied Earth Observation and Geoinformation  
648 23:344–351.
- 649 Coops, N. C., M. Johnson, M. A. Wulder, and J. C. White. 2006. Assessment of QuickBird high spatial  
650 resolution imagery to detect red attack damage due to mountain pine beetle infestation. Remote Sensing of  
651 Environment 103:67–80.
- 652 DJI. 2015a. Zenmuse X3 - Creativity Unleashed. <https://www.dji.com/zenmuse-x3/info>.
- 653 DJI. 2015b. DJI - The World Leader in Camera Drones/Quadcopters for Aerial Photography. <https://www.dji.com/matrice100/info>.
- 655 DronesMadeEasy. 2018. Map Pilot for DJI on iOS. [https://itunes.apple.com/us/app/map-pilot-for-dji/  
656 id1014765000?mt=8](https://itunes.apple.com/us/app/map-pilot-for-dji/id1014765000?mt=8).
- 657 Evenden, M. L., C. M. Whitehouse, and J. Sykes. 2014. Factors influencing flight capacity of the mountain  
658 pine beetle (Coleoptera: Curculionidae: Scolytinae). Environmental Entomology 43:187–196.
- 659 Eysn, L., M. Hollaus, E. Lindberg, F. Berger, J.-M. Monnet, M. Dalponte, M. Kobal, M. Pellegrini, E.  
660 Lingua, D. Mongus, and N. Pfeifer. 2015. A benchmark of LiDAR-based single tree detection methods using  
661 heterogeneous forest data from the alpine space. Forests 6:1721–1747.
- 662 Farr, T. G., P. A. Rosen, E. Caro, R. Crippen, R. Duren, S. Hensley, M. Kobrick, M. Paller, E. Rodriguez, L.  
663 Roth, D. Seal, S. Shaffer, J. Shimada, J. Umland, M. Werner, M. Oskin, D. Burbank, and D. Alsdorf. 2007.  
664 The shuttle radar topography mission. Reviews of Geophysics 45.
- 665 Fettig, C. J. 2012. Chapter 2: Forest health and bark beetles. *in* Managing Sierra Nevada Forests. PSW-  
666 GTR-237. USDA Forest Service.

- 667 Fettig, C. J. 2016. Native bark beetles and wood borers in Mediterranean forests of California. Pages 499–528  
668 *in* Insects and diseases of Mediterranean Forest systems. Springer International Publishing, Switzerland.
- 669 Fettig, C. J., C. P. Dabney, S. R. McKelvey, and D. P. W. Huber. 2008. Nonhost angiosperm volatiles and  
670 verbenone protect individual ponderosa pines from attack by western pine beetle and red turpentine beetle  
671 (Coleoptera: Curculionidae, Scolytinae). *Western Journal of Applied Forestry* 23:40–45.
- 672 Fettig, C. J., and J. Hilszczański. 2015. Management strategies for bark beetles in conifer forests. Pages  
673 555–584 *in* Bark Beetles. Elsevier.
- 674 Fettig, C. J., K. D. Klepzig, R. F. Billings, A. S. Munson, T. E. Nebeker, J. F. Negrón, and J. T. Nowak. 2007.  
675 The effectiveness of vegetation management practices for prevention and control of bark beetle infestations in  
676 coniferous forests of the western and southern United States. *Forest Ecology and Management* 238:24–53.
- 677 Fettig, C. J., S. R. McKelvey, C. P. Dabney, D. P. W. Huber, C. G. Lait, D. L. Fowler, and J. H. Borden. 2012.  
678 Efficacy of “Verbenone Plus” for protecting ponderosa pine trees and stands from *Dendroctonus brevicomis*  
679 (Coleoptera: Curculionidae) attack in British Columbia and California. *Journal of Economic Entomology*  
680 105:1668–1680.
- 681 Fettig, C. J., S. R. McKelvey, and D. P. W. Huber. 2005. Nonhost angiosperm volatiles and Verbenone disrupt  
682 response of western pine beetle, *Dendroctonus brevicomis* (Coleoptera: Scolytidae), to attractant-baited traps.  
683 *Journal of Economic Entomology* 98:2041–2048.
- 684 Fettig, C. J., L. A. Mortenson, B. M. Bulaon, and P. B. Foulk. 2019. Tree mortality following drought in the  
685 central and southern Sierra Nevada, California, U.S. *Forest Ecology and Management* 432:164–178.
- 686 Flint, L. E., A. L. Flint, J. H. Thorne, and R. Boynton. 2013. Fine-scale hydrologic modeling for regional land-  
687 scape applications: The California Basin Characterization Model development and performance. *Ecological  
688 Processes* 2:25.
- 689 Floyd, M. L., M. Clifford, N. S. Cobb, D. Hanna, R. Delph, P. Ford, and D. Turner. 2009. Relationship of  
690 stand characteristics to drought-induced mortality in three Southwestern piñonJuniper woodlands. *Ecological  
691 Applications* 19:1223–1230.
- 692 Franceschi, V. R., P. Krokene, E. Christiansen, and T. Krekling. 2005. Anatomical and chemical defenses of  
693 conifer bark against bark beetles and other pests. *New Phytologist* 167:353–376.
- 694 Frey, J., K. Kovach, S. Stemmler, and B. Koch. 2018. UAV photogrammetry of forests as a vulnerable  
695 process. A sensitivity analysis for a structure from motion RGB-image pipeline. *Remote Sensing* 10:912.

- 696 Fricker, G. A., N. W. Synes, J. M. Serra-Diaz, M. P. North, F. W. Davis, and J. Franklin. 2019. More than  
697 climate? Predictors of tree canopy height vary with scale in complex terrain, Sierra Nevada, CA (USA).  
698 *Forest Ecology and Management* 434:142–153.
- 699 Gabry, J., D. Simpson, A. Vehtari, M. Betancourt, and A. Gelman. 2019. Visualization in Bayesian workflow.  
700 *Journal of the Royal Statistical Society: Series A (Statistics in Society)* 182:389–402.
- 701 Geiszler, D. R., and R. I. Gara. 1978. Mountain pine beetle attack dynamics in lodgepole pine. *in Theory*  
702 *and Practice of Mountain Pine Beetle Management in Lodgepole Pine Forests: Symposium Proceedings*. A.  
703 A. Berryman, G. D. Amman and R. W. Stark (Eds). Pullman, WA, USA.
- 704 Gitelson, A., and M. N. Merzlyak. 1994. Spectral reflectance changes associated with autumn senescence of  
705 *Aesculus hippocastanum* L. And *Acer platanoides* L. Leaves. Spectral features and relation to chlorophyll  
706 estimation. *Journal of Plant Physiology* 143:286–292.
- 707 Graf, M., M. Reid, B. Aukema, and B. Lindgren. 2012. Association of tree diameter with body size and lipid  
708 content of mountain pine beetles. *The Canadian Entomologist* 144:467–477.
- 709 Gray, P. C., A. B. Fleishman, D. J. Klein, M. W. McKown, V. S. Bézy, K. J. Lohmann, and D. W. Johnston.  
710 2019. A convolutional neural network for detecting sea turtles in drone imagery. *Methods in Ecology and*  
711 *Evolution* 10:345–355.
- 712 Griffin, D., and K. J. Anchukaitis. 2014. How unusual is the 2012-2014 California drought? *Geophysical*  
713 *Research Letters* 41:9017–9023.
- 714 Hayes, C. J., C. J. Fettig, and L. D. Merrill. 2009. Evaluation of multiple funnel traps and stand characteristics  
715 for estimating western pine beetle-caused tree mortality. *Journal of Economic Entomology* 102:2170–2182.
- 716 Hijmans, R. J., J. van Etten, M. Sumner, J. Cheng, A. Bevan, R. Bivand, L. Busetto, M. Canty, D. Forrest,  
717 A. Ghosh, D. Golicher, J. Gray, J. A. Greenberg, P. Hiemstra, I. for M. A. Geosciences, C. Karney, M.  
718 Mattiuzzi, S. Mosher, J. Nowosad, E. Pebesma, O. P. Lamigueiro, E. B. Racine, B. Rowlingson, A. Shortridge,  
719 B. Venables, and R. Wueest. 2019. *Raster: Geographic data analysis and modeling*.
- 720 Hoffman, M. D., and A. Gelman. 2014. The No-U-Turn Sampler: Adaptively setting path lengths in  
721 Hamiltonian Monte Carlo. *Journal of Machine Learning Research* 15:31.
- 722 Hunziker, P. 2017. *Velox: Fast raster manipulation and extraction*.
- 723 Jactel, H., and E. G. Brockerhoff. 2007. Tree diversity reduces herbivory by forest insects. *Ecology Letters*  
724 10:835–848.

- 725 Jakubowski, M. K., W. Li, Q. Guo, and M. Kelly. 2013. Delineating individual trees from LiDAR data: A  
726 comparison of vector- and raster-based segmentation approaches. *Remote Sensing* 5:4163–4186.
- 727 James, M. R., and S. Robson. 2014. Mitigating systematic error in topographic models derived from UAV  
728 and ground-based image networks. *Earth Surface Processes and Landforms* 39:1413–1420.
- 729 Jeronimo, S. M. A., V. R. Kane, D. J. Churchill, J. A. Lutz, M. P. North, G. P. Asner, and J. F. Franklin.  
730 2019. Forest structure and pattern vary by climate and landform across active-fire landscapes in the montane  
731 Sierra Nevada. *Forest Ecology and Management* 437:70–86.
- 732 Kaiser, K. E., B. L. McGlynn, and R. E. Emanuel. 2013. Ecohydrology of an outbreak: Mountain pine beetle  
733 impacts trees in drier landscape positions first. *Ecohydrology* 6:444–454.
- 734 Kane, V. R., M. P. North, J. A. Lutz, D. J. Churchill, S. L. Roberts, D. F. Smith, R. J. McGaughey, J. T.  
735 Kane, and M. L. Brooks. 2014. Assessing fire effects on forest spatial structure using a fusion of Landsat and  
736 airborne LiDAR data in Yosemite National Park. *Remote Sensing of Environment* 151:89–101.
- 737 Klein, W. H., D. L. Parker, and C. E. Jensen. 1978. Attack, emergence, and stand depletion trends of the  
738 mountain pine beetle in a lodgepole pine stand during an outbreak. *Environmental Entomology* 7:732–737.
- 739 Kolb, T. E., C. J. Fettig, M. P. Ayres, B. J. Bentz, J. A. Hicke, R. Mathiasen, J. E. Stewart, and A. S. Weed.  
740 2016. Observed and anticipated impacts of drought on forest insects and diseases in the United States. *Forest  
741 Ecology and Management* 380:321–334.
- 742 Kuhn, M. 2008. Building predictive models in R using the caret package. *Journal of Statistical Software*  
743 28:1–26.
- 744 Larson, A. J., and D. Churchill. 2012. Tree spatial patterns in fire-frequent forests of western North America,  
745 including mechanisms of pattern formation and implications for designing fuel reduction and restoration  
746 treatments. *Forest Ecology and Management* 267:74–92.
- 747 Li, W., Q. Guo, M. K. Jakubowski, and M. Kelly. 2012. A new method for segmenting individual trees from  
748 the LiDAR point cloud. *Photogrammetric Engineering & Remote Sensing* 78:75–84.
- 749 Logan, J. A., P. White, B. J. Bentz, and J. A. Powell. 1998. Model analysis of spatial patterns in mountain  
750 pine beetle outbreaks. *Theoretical Population Biology* 53:236–255.
- 751 Ma, S., A. Concilio, B. Oakley, M. North, and J. Chen. 2010. Spatial variability in microclimate in a  
752 mixed-conifer forest before and after thinning and burning treatments. *Forest Ecology and Management*  
753 259:904–915.

- 754 McDowell, N., W. T. Pockman, C. D. Allen, D. D. Breshears, N. Cobb, T. Kolb, J. Plaut, J. Sperry, A. West,  
755 D. G. Williams, and E. A. Yepez. 2008. Mechanisms of plant survival and mortality during drought: Why do  
756 some plants survive while others succumb to drought? *New Phytologist* 178:719–739.
- 757 Meyer, F., and S. Beucher. 1990. Morphological segmentation. *Journal of Visual Communication and Image  
758 Representation* 1:21–46.
- 759 Micasense. 2015. MicaSense. <https://support.micasense.com/hc/en-us/articles/215261448-RedEdge-User->  
760 Manual-PDF-Download-.
- 761 Millar, C. I., N. L. Stephenson, and S. L. Stephens. 2007. Climate change and forests of the future: Managing  
762 in the face of uncertainty. *Ecological Applications* 17:2145–2151.
- 763 Millar, C. I., R. D. Westfall, D. L. Delany, M. J. Bokach, A. L. Flint, and L. E. Flint. 2012. Forest mortality in  
764 high-elevation whitebark pine (*Pinus albicaulis*) forests of eastern California, USA: Influence of environmental  
765 context, bark beetles, climatic water deficit, and warming. *Canadian Journal of Forest Research* 42:749–765.
- 766 Miller, J. M., and F. P. Keen. 1960. Biology and control of the western pine beetle: A summary of the first  
767 fifty years of research. US Department of Agriculture.
- 768 Mitchell, R. G., and H. K. Preisler. 1991. Analysis of spatial patterns of lodgepole pine attacked by outbreak  
769 populations of the mountain pine beetle. *Forest Science* 37:1390–1408.
- 770 Moeck, H. A., D. L. Wood, and K. Q. Lindahl. 1981. Host selection behavior of bark beetles (Coleoptera:  
771 Scolytidae) attacking *Pinus ponderosa*, with special emphasis on the western pine beetle, *Dendroctonus*  
772 *brevicomis*. *Journal of Chemical Ecology* 7:49–83.
- 773 Morris, J. L., S. Cottrell, C. J. Fettig, W. D. Hansen, R. L. Sherriff, V. A. Carter, J. L. Clear, J. Clement, R.  
774 J. DeRose, J. A. Hicke, P. E. Higuera, K. M. Mattor, A. W. R. Seddon, H. T. Seppä, J. D. Stednick, and S.  
775 J. Seybold. 2017. Managing bark beetle impacts on ecosystems and society: Priority questions to motivate  
776 future research. *Journal of Applied Ecology* 54:750–760.
- 777 Oliver, W. W. 1995. Is self-thinning in ponderosa pine ruled by *Dendroctonus* bark beetles? Page 6 *in* Forest  
778 health through silviculture: Proceedings of the 1995 National Silviculture Workshop.
- 779 Pau, G., F. Fuchs, O. Sklyar, M. Boutros, and W. Huber. 2010. EBImage: An R package for image processing  
780 with applications to cellular phenotypes. *Bioinformatics* 26:979–981.
- 781 Person, H. L. 1928. Tree selection by the western pine beetle. *Journal of Forestry* 26:564–578.
- 782 Person, H. L. 1931. Theory in explanation of the selection of certain trees by the western pine beetle. *Journal*

- 783 of Forestry 29:696–699.
- 784 Pile, L. S., M. D. Meyer, R. Rojas, O. Roe, and M. T. Smith. 2019. Drought impacts and compounding  
785 mortality on forest trees in the southern Sierra Nevada. Forests 10:237.
- 786 Plowright, A. 2018. ForestTools: Analyzing remotely sensed forest data.
- 787 Preisler, H. K. 1993. Modelling spatial patterns of trees attacked by bark-beetles. Applied Statistics 42:501.
- 788 Raffa, K. F., B. H. Aukema, B. J. Bentz, A. L. Carroll, J. A. Hicke, M. G. Turner, and W. H. Romme. 2008.  
789 Cross-scale drivers of natural disturbances prone to anthropogenic amplification: The dynamics of bark beetle  
790 eruptions. BioScience 58:501–517.
- 791 Raffa, K. F., and A. A. Berryman. 1983. The role of host plant resistance in the colonization behavior and  
792 ecology of bark beetles (Coleoptera: Scolytidae). Ecological Monographs 53:27–49.
- 793 Raffa, K. F., and A. A. Berryman. 1987. Interacting selective pressures in conifer-bark beetle systems: A  
794 basis for reciprocal adaptations? The American Naturalist 129:234–262.
- 795 Raffa, K. F., J.-C. Grégoire, and B. Staffan Lindgren. 2015. Natural history and ecology of bark beetles.  
796 Pages 1–40 *in* Bark Beetles. Elsevier.
- 797 R Core Team. 2018. R: A language and environment for statistical computing. R Foundation for Statistical  
798 Computing, Vienna, Austria.
- 799 Restaino, C., D. Young, B. Estes, S. Gross, A. Wuenschel, M. Meyer, and H. Safford. 2019. Forest  
800 structure and climate mediate drought-induced tree mortality in forests of the Sierra Nevada, USA. Ecological  
801 Applications 0:e01902.
- 802 Robeson, S. M. 2015. Revisiting the recent California drought as an extreme value. Geophysical Research  
803 Letters 42:6771–6779.
- 804 Rouse, W., R. H. Haas, W. Deering, and J. A. Schell. 1973. Monitoring the vernal advancement and  
805 retrogradation (green wave effect) of natural vegetation. Type II Report, Goddard Space Flight Center,  
806 Greenbelt, MD, USA.
- 807 Roussel, J.-R. 2019. lidRplugins: Extra functions and algorithms for lidR package.
- 808 Roussel, J.-R., D. Auty, F. De Boissieu, and A. S. Meador. 2019. lidR: Airborne LiDAR data manipulation  
809 and visualization for forestry applications.
- 810 Safford, H. D., and J. T. Stevens. 2017. Natural range of variation for yellow pine and mixed-conifer forests

- 811 in the Sierra Nevada, Southern Cascades, and Modoc and Inyo National Forests, California, USA. Page 241.
- 812 dos Santos, A. A., J. Marcato Junior, M. S. Araújo, D. R. Di Martini, E. C. Tetila, H. L. Siqueira, C. Aoki, A.
- 813 Eltner, E. T. Matsubara, H. Pistori, R. Q. Feitosa, V. Liesenberg, and W. N. Gonçalves. 2019. Assessment of
- 814 CNN-Based Methods for Individual Tree Detection on Images Captured by RGB Cameras Attached to UAVs.
- 815 Sensors (Basel, Switzerland) 19.
- 816 Seidl, R., J. Müller, T. Hothorn, C. Bässler, M. Heurich, and M. Kautz. 2016. Small beetle, large-scale
- 817 drivers: How regional and landscape factors affect outbreaks of the European spruce bark beetle. The Journal
- 818 of Applied Ecology 53:530–540.
- 819 Senf, C., E. M. Campbell, D. Pflugmacher, M. A. Wulder, and P. Hostert. 2017. A multi-scale analysis of
- 820 western spruce budworm outbreak dynamics. Landscape Ecology 32:501–514.
- 821 Seybold, S. J., B. J. Bentz, C. J. Fettig, J. E. Lundquist, R. A. Progar, and N. E. Gillette. 2018. Management
- 822 of western North American bark beetles with semiochemicals. Annual Review of Entomology 63:407–432.
- 823 Shepherd, W. P., D. P. W. Huber, S. J. Seybold, and C. J. Fettig. 2007. Antennal responses of the western
- 824 pine beetle, *Dendroctonus brevicomis* (Coleoptera: Curculionidae), to stem volatiles of its primary host, *Pinus*
- 825 *ponderosa*, and nine sympatric nonhost angiosperms and conifers. Chemoecology 17:209–221.
- 826 Shiklomanov, A. N., B. A. Bradley, K. M. Dahlin, A. M. Fox, C. M. Gough, F. M. Hoffman, E. M. Middleton,
- 827 S. P. Serbin, L. Smallman, and W. K. Smith. 2019. Enhancing global change experiments through integration
- 828 of remote-sensing techniques. Frontiers in Ecology and the Environment 0.
- 829 Shin, P., T. Sankey, M. Moore, and A. Thode. 2018. Evaluating unmanned aerial vehicle images for estimating
- 830 forest canopy fuels in a ponderosa pine stand. Remote Sensing 10:1266.
- 831 Stephenson, N. 1998. Actual evapotranspiration and deficit: Biologically meaningful correlates of vegetation
- 832 distribution across spatial scales. Journal of Biogeography 25:855–870.
- 833 Stephenson, N. L., A. J. Das, N. J. Ampersee, and B. M. Bulaon. 2019. Which trees die during drought?
- 834 The key role of insect host-tree selection. Journal of Ecology 75:2383–2401.
- 835 Stovall, A. E. L., H. Shugart, and X. Yang. 2019. Tree height explains mortality risk during an intense
- 836 drought. Nature Communications 10:1–6.
- 837 Thistle, H. W., H. Peterson, G. Allwine, B. Lamb, T. Strand, E. H. Holsten, and P. J. Shea. 2004. Surrogate
- 838 pheromone plumes in three forest trunk spaces: Composite statistics and case studies. Forest Science 50.
- 839 USDAFS. 2017, December 12. Press Release: Record 129 million dead trees in California. <https://www.fs.fed.us>.

- 840 usda.gov/Internet/FSE\_DOCUMENTS/fseprd566303.pdf.
- 841 USDAFS. 2019, February 11. Press Release: Survey finds 18 million trees died in California in 2018.
- 842 [https://www.fs.usda.gov/Internet/FSE\\_DOCUMENTS/FSEPRD609321.pdf](https://www.fs.usda.gov/Internet/FSE_DOCUMENTS/FSEPRD609321.pdf).
- 843 Vega, C., A. Hamrouni, S. El Mokhtari, J. Morel, J. Bock, J. P. Renaud, M. Bouvier, and S. Durrieu. 2014.
- 844 PTrees: A point-based approach to forest tree extraction from LiDAR data. International Journal of Applied
- 845 Earth Observation and Geoinformation 33:98–108.
- 846 Vose, J. M., D. L. Peterson, G. M. Domke, C. J. Fettig, L. Joyce, R. E. Keane, C. H. Luce, J. P. Prestemon,
- 847 L. E. Band, J. S. Clark, N. E. Cooley, A. D'Amato, and J. E. Halofsky. 2018. Forests. In Impacts, Risks,
- 848 and Adaptation in the United States: The Fourth National Climate Assessment, Volume II [Reidmiller, D.
- 849 R., C. W. Avery, D. R. Easterling, K. E. Kunkel, K. L. M. Lewis, T. K. Maycock, and B. C. Stewart (eds.)].
- 850 Pages 232–267. U.S. Global Change Research Program.
- 851 Wallin, K. F., and K. F. Raffa. 2004. Feedback between individual host selection behavior and population
- 852 dynamics in an eruptive herbivore. Ecological Monographs 74:101–116.
- 853 Waring, R. H., and G. B. Pitman. 1985. Modifying lodgepole pine stands to change susceptibility to mountain
- 854 pine beetle attack. Ecology 66:889–897.
- 855 Weinstein, B. G., S. Marconi, S. Bohlman, A. Zare, and E. White. 2019. Individual tree-crown detection in
- 856 RGB imagery using semi-supervised deep learning neural networks. Remote Sensing 11:1309.
- 857 Wyngaard, J., L. Barbieri, A. Thomer, J. Adams, D. Sullivan, C. Crosby, C. Parr, J. Klump, S. Raj Shrestha,
- 858 and T. Bell. 2019. Emergent challenges for science sUAS data management: Fairness through community
- 859 engagement and best practices development. Remote Sensing 11:1797.
- 860 Young, D. J. N., J. T. Stevens, J. M. Earles, J. Moore, A. Ellis, A. L. Jirka, and A. M. Latimer. 2017.
- 861 Long-term climate and competition explain forest mortality patterns under extreme drought. Ecology Letters
- 862 20:78–86.
- 863 Zhang, W., J. Qi, P. Wan, H. Wang, D. Xie, X. Wang, and G. Yan. 2016. An easy-to-use airborne LiDAR
- 864 data filtering method based on cloth simulation. Remote Sensing 8:501.